# Human infrared vision is triggered by two-photon chromophore isomerization

Grazyna Palczewska[a,1], Frans Vinberg[b,1], Patrycjusz Stremplewski[c,1], Martin P. Bircher[d], David Salom[e], Katarzyna Komar[c], Jianye Zhang[e], Michele Cascella[f,2], Maciej Wojtkowski[c,2], Vladimir J. Kefalov[b,2], and Krzysztof Palczewski[e,2]

[a]Department of Medical Devices, Polgenix, Inc., Cleveland, OH 44106; [b]Ophthalmology and Visual Sciences, Washington University School of Medicine, St. Louis, MO 63110; [c]Faculty of Physics, Astronomy and Informatics, Institute of Physics, Nicolaus Copernicus University, 87-100 Torun, Poland; [d]Department of Chemistry and Biochemistry, University of Bern, CH-3012 Bern, Switzerland; [e]Department of Pharmacology, Cleveland Center for Membrane and Structural Biology, School of Medicine, Case Western Reserve University, Cleveland, OH 44106; and [f]Department of Chemistry and Centre for Theoretical and Computational Chemistry, University of Oslo, N-0315 Oslo, Norway

Edited by Austin Roorda, University of California, Berkeley, CA, and accepted by the Editorial Board October 30, 2014 (received for review June 3, 2014)

**Vision relies on photoactivation of visual pigments in rod and cone photoreceptor cells of the retina. The human eye structure and the absorption spectra of pigments limit our visual perception of light. Our visual perception is most responsive to stimulating light in the 400- to 720-nm (visible) range. First, we demonstrate by psychophysical experiments that humans can perceive infrared laser emission as visible light. Moreover, we show that mammalian photoreceptors can be directly activated by near infrared light with a sensitivity that paradoxically increases at wavelengths above 900 nm, and display quadratic dependence on laser power, indicating a nonlinear optical process. Biochemical experiments with rhodopsin, cone visual pigments, and a chromophore model compound 11-*cis*-retinyl-propylamine Schiff base demonstrate the direct isomerization of visual chromophore by a two-photon chromophore isomerization. Indeed, quantum mechanics modeling indicates the feasibility of this mechanism. Together, these findings clearly show that human visual perception of near infrared light occurs by two-photon isomerization of visual pigments.**

visual pigment | two-photon absorption | rhodopsin | transretinal electrophysiology | multiscale modeling

Human vision is generally believed to be restricted to a visible light range, although >50% of the sun's radiation energy that reaches earth is in the infrared (IR) range (1). Human rod and cone visual pigments with the 11-*cis*-retinylidene chromophore absorb in the visible range, with absorption monotonically declining from their maxima of 430–560 nm toward longer wavelengths. The spectral sensitivity of human dim light perception matches well with the absorption spectrum of the rod visual pigment, rhodopsin (2, 3). Activation of visual pigments is temperature independent around their absorption peaks ($\lambda_{max}$), but at longer wavelengths, the lower energy photons must be supplemented by heat to achieve chromophore photoisomerization (4). Long wavelength-sensitive visual pigments of vertebrates exhibit maximal absorption at the ∼500- to ∼625-nm range. Pigments with $\lambda_{max} > 700$ nm are theoretically possible, but the high noise due to spontaneous thermal activation would render them impractical (5). At human body temperature and with 1,050-nm stimulation, the sensitivity of the peripheral retina to one-photon (1PO) stimulation is less than $10^{-12}$ of its maximum value at 505 nm (4, 6). Indeed, reports about human IR vision can be found in the literature, although they are fragmentary and do not describe the mechanism of this phenomenon.

With the invention of radar during World War II, it was immediately questioned if pilots could detect high intensity radiation in the IR range of the spectrum. Wald and colleagues reported that at wavelengths above 800 nm, rod photoreceptors become more sensitive than cones, resulting in perception of IR signals as white light selectively in the peripheral retina (6). They proposed that relative spectral sensitivity declines monotonically toward longer wavelengths to below the $10^{-12}$ level at 1,050 nm compared with its peak at 505 nm (7). With more advanced sources of IR light, it was found that rods and cones of the retina could respond to radiation at wavelengths of as long as 1,355 nm (6, 8–10). Suggested mechanisms included second harmonic generation (SHG) (11) in the eye, fluorescence, and two-photon (2PO) absorption (12) in the retina. Several electrophysiological studies with lower vertebrate photoreceptors provided an indication for a nonlinear optical process involved in activation of rhodopsin (13, 14). However, these studies did not probe the mechanism, and, more importantly, their implications for mammalian visual pigment activation and human vision remained unclear. The retinal SHG hypothesis appeared scientifically sound in the context of published results demonstrating that all-*trans*-retinal loaded in the plasma membrane can serve as a source of an SHG signal (14). One argument claimed by Walraven et al. (11) in favor of SHG vs. 2PO absorption was that rhodopsin should fluoresce at longer wavelengths if excited by a 2PO absorption mechanism, leading to a red shift in visual perception (11). Rhodopsin indeed is a fluorophore, but its quantum yield is only $\sim 10^{-5}$ (15), making this last explanation unlikely. Thus, the true mechanism of IR visual sensation has remained unidentified.

## Significance

This study resolves a long-standing question about the ability of humans to perceive near infrared radiation (IR) and identifies a mechanism driving human IR vision. A few previous reports and our expanded psychophysical studies here reveal that humans can detect IR at wavelengths longer than 1,000 nm and perceive it as visible light, a finding that has not received a satisfactory physical explanation. We show that IR light activates photoreceptors through a nonlinear optical process. IR light also caused photoisomerization of purified pigments and a model chromophore compound. These observations are consistent with our quantum mechanical model for the energetics of two-photon activation of rhodopsin. Thus, humans can perceive IR light via two-photon isomerization of visual pigment chromophores.

Author contributions: G.P., F.V., P.S., M.P.B., D.S., K.K., M.C., M.W., V.J.K., and K.P. designed research; G.P., F.V., P.S., M.P.B., D.S., K.K., J.Z., M.C., and V.J.K. performed research; J.Z. contributed new reagents/analytic tools; G.P., P.S., M.P.B., D.S., K.K., J.Z., M.C., M.W., V.J.K., and K.P. analyzed data; and G.P., F.V., D.S., K.K., M.C., M.W., V.J.K., and K.P. wrote the paper.

The authors declare no conflict of interest.

This article is a PNAS Direct Submission. A.R. is a guest editor invited by the Editorial Board.

[1]G.P., F.V., and P.S. contributed equally to this work.

[2]To whom correspondence may be addressed. Email: michele.cascella@kjemi.uio.no, max@fizyka.umk.pl, kefalov@vision.wustl.edu, or kxp65@case.edu.

This article contains supporting information online at www.pnas.org/lookup/suppl/doi:10.1073/pnas.1410162111/-/DCSupplemental.

By combining modern optical, electrophysiological, biochemical, and computational tools with psychophysical experiments, we report here that humans can see IR radiation through 2PO absorption and direct photoisomerization of visual pigment molecules in rod and cone photoreceptor cells.

## Results

**Humans Can Detect IR Light.** Some authors of the present paper perceived low energy IR laser radiation of 1,060 nm as a pale greenish light. This novel experience engaged our interest in understanding the fundamental mechanism of human IR vision. To test whether a nonlinear optical process was involved, we exposed human eyes to 1 mW of pulsed laser radiation at 1,040 nm and observed that green light perception was much stronger for pulsed light compared with CW (continuous wave) light of the same average power. Using a laser delivering 200-fs, 76-MHz excitation light, we were able to obtain consistent visible light sensation, strong enough to perform accurate color matching experiments. Using the experimental setup depicted in Fig. 1*A*, we then tested human visual responses to IR light. Fig. 1*B* shows the results of matching wavelengths of visible radiation to visual perception produced by an IR beam scanning the retinas of 30 healthy volunteers. All tested subjects detected the IR light. The data could be fit well with a linear function (solid line). The deviation from the frequency-doubled wavelength was noticeably larger for the points produced by 1,020- and 1,040-nm stimuli. These two well-perceived wavelengths also featured the largest SDs, with the exception of 1,200 nm, where light perception was very weak due to increased absorption by water (16). These results suggest 2PO excitation or SHG as a mechanism contributing to visual color perception of IR light. If the SHG process was the only mechanism causing the perception of IR radiation as visible light, then the spectral width of the generated radiation should be roughly the same for every wavelength and coincide with the spectral width of the monochromator output, which transmits an 8-nm spectral bandwidth. This feature was observed for 950, 975, 1,125, and 1,150 nm, with SDs for these wavelengths at 7.2, 8.5, 7.4, and 8 nm, respectively, but not for 1,020- and 1,040-nm stimuli that had greater SDs (~12 nm). There are also other factors potentially influencing hue perception in color matching experiments, e.g., the Stiles–Crawford effect of the second kind (17).

The reproducibility of our experiments was tested in two healthy volunteers (subjects 1 and 2) with a procedure of matching double frequency wavelength for 1,040 nm repeated 10 times. Testing of subjects 1 and 2 was performed with a 0.9-mW IR light beam; tests of subject 1 were done additionally with 0.44- and 0.12-mW light beams (Fig. 1*C*). For higher powers of the applied laser beam, the perceived color seemed to be slightly red shifted. This observation could be explained by the additional contribution of red-shifted weak fluorescent light more easily detectable at increased optical power; however, this secondary absorption of emitted fluorescence could also occur in a 1PO excitation process.

To further investigate the nonlinearity of visual excitation, we conducted measurements of sensitivity to IR radiation (Fig. 2) using 0.3- to 0.6-ns (long) and 0.5- to 1.25-ps (short) laser pulses in two healthy subjects. We defined sensitivity as the reciprocal of the minimal power of the laser beam that still causes visual sensation. The beam was scanned horizontally at the fovea's height. For long pulses and wavelengths shorter than 1,000 nm, our sensitivity results agreed with those obtained by Wald's group (6). We found the deviation from a monotonic decrease in sensitivity for wavelengths longer than 1,000 nm. For excitation wavelengths shorter than 1,040 nm, the perceived color of light was red. For excitation wavelengths longer than 1,040 nm, the perceived color matched about half of the excitation wavelength. Wald's curve terminated at 1,000 nm for the fovea and at 1,050 nm for the peripheral retina, showing further decrease at 1,050 nm equal to half an order of magnitude.

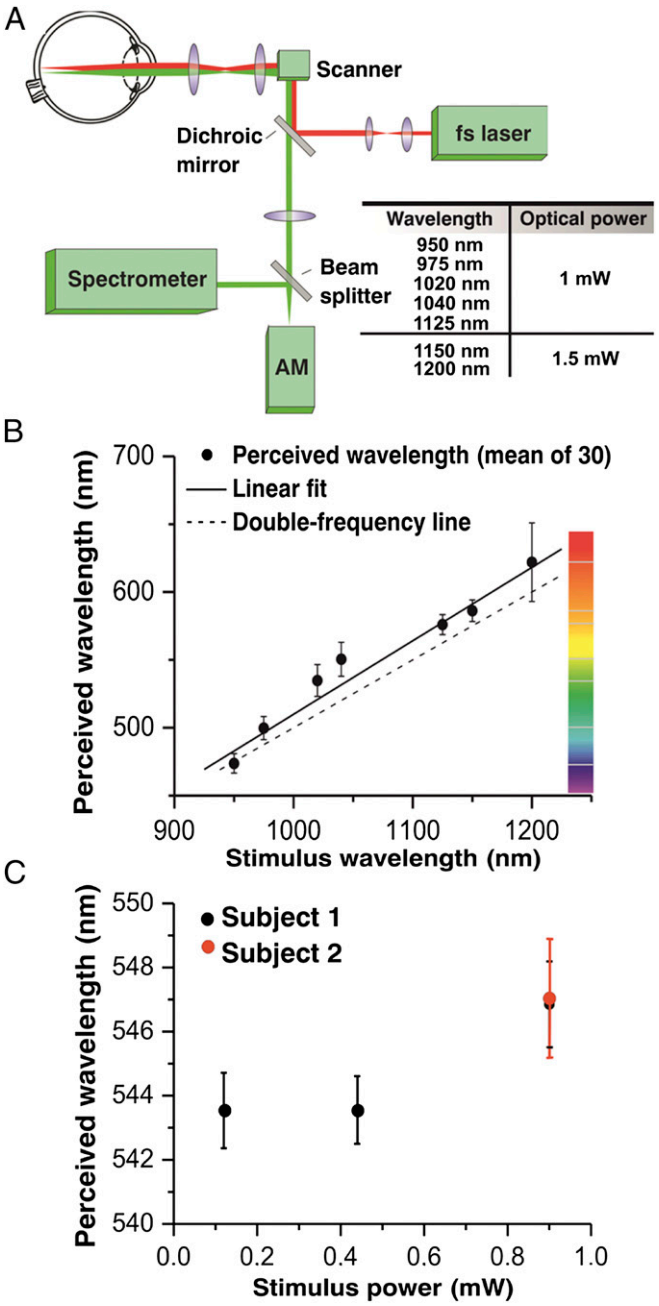


**Fig. 1.** Color perception caused by IR laser radiation of the human eye in vivo. (*A*) Experimental optical setup. AM, adjustable monochromator. (*B*) Plot showing the results of matching frequency-doubled wavelength perception with the true visible radiation illuminating the retina for 30 healthy volunteers. (*C*) Reproducibility of results obtained from two healthy volunteers (subjects 1 and 2) for different beam powers at 1,040 nm. Points plotted on the graph represent means of matching wavelengths performed by all examined subjects. Error bars in *B* represent SDs of adjusted wavelengths. Error bars in *C* are SDs of the means.

For short pulses, we found that changing the wavelength from 800 to 900 nm resulted in a decrease of sensitivity by ~3 orders of magnitude from $3.4 \times 10^7$ to $9.9 \times 10^4$ $W^{-1}$ for subject 1 and from $2 \times 10^8$ to $7.9 \times 10^5$ $W^{-1}$ for subject 2. This result is consistent with Wald and colleagues (7) who found a decrease of sensitivity by 2.5 orders of magnitude for these wavelengths. For 1,000 nm,

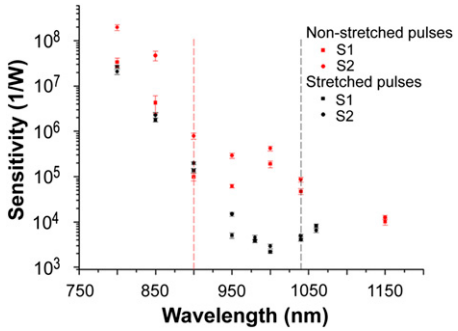


**Fig. 2.** A nonlinear process contributes to spectral sensitivity of human visual perception. Spectral sensitivity data obtained with 0.3- to 0.6-ns (long) laser pulses are shown in black and the spectral sensitivity data obtained with 0.5- to 1.25-ps (short) laser pulses are in red. Dashed vertical lines separate regions of wavelengths with different color perception. Measurements were taken on two healthy dark-adapted subjects (S1 and S2). Each point represents the average of 10 measurements.

Wald's group found a further decrease of sensitivity amounting to ~1.7 orders of magnitude (averaging fovea and periphery); our measurements for this wavelength show an increase of sensitivity to $19 \times 10^4$ W$^{-1}$ in subject 1 and only a slight decrease to $4.2 \times 10^5$ W$^{-1}$ for subject 2 (Fig. 2). For excitation wavelengths shorter than 900 nm, the perceived color of light was red. For excitation wavelengths 950 nm and longer, the perceived color matched roughly half of the excitation wavelength.

To quantify the impact of a nonlinear process on inducing visual sensation, we varied the duty cycle by changing the laser pulse duration while keeping the pulse repetition frequency constant. We compared the minimum laser power needed for inducing visual sensation (sensitivity) when using long pulses with ~0.5-ns duration to that needed when using short pulses of ~0.9-ps duration (Fig. 2). Around 1,000 nm (a region where a green light was perceived for short pulses and reddish for long pulses), the minimum laser power needed to evoke perception of light was more than 100 times larger for long pulses (on average $0.4 \times 10^{-3}$ W) than that needed for short pulses (on average $0.3 \times 10^{-5}$ W). This more than 100-fold increase in required laser power indicates the involvement of nonlinear processes in evoking IR light perception by the human eye. At wavelengths shorter than 900 nm, the difference in sensitivity to long and short pulses was small, indicating that a 1PO process is predominant for both long and short pulses in this region of wavelengths. Considering that absorption of IR by ocular tissue increases with increasing wavelengths (18), our results also show the optimal region, just above 1,040 nm, for the human eye to perceive IR as light with colors corresponding to roughly half of the excitation wavelengths.

These two sets of results indicate that, depending on wavelengths, pulse duration, and laser power, we observed a combined effect of different physical processes: 1PO excitation, 2PO excitation, and perhaps SHG.

The above experiments were performed with foveal stimulation of the tested subjects and produced a color visual sensation, indicating that cones mediate IR vision.

To verify whether this process pertains to rods as well, we performed our visual tests on a person with documented autosomal recessive achromatopsia (ACHM) (19). This individual also perceived IR beams of 950- and 1,040-nm wavelengths. Here, visual perception was monochromatic, demonstrating the ability of human rods to detect IR light.

**Mouse Photoreceptors Respond to IR Light.** Both sclera and cornea are sources of SHG signals (20, 21). Considering that our data on human subjects did not exclude a contribution of SHG to IR vision, we measured light responses directly from photoreceptors in intact retinas isolated from mouse eyes [transretinal electroretinograms (ERGs); *Methods*] (22). Here photoreceptors were exposed directly to IR light without interference from the cornea and lens, thereby avoiding external sources of SHG light. We also used the mouse retina to take advantage of genetic tools for identifying the source of the IR-evoked signal. Photoreceptor responses were first recorded from dark-adapted WT mouse retinas exposed to light from a laser delivering 75-fs light pulses at an 80-MHz repetition frequency and wavelengths ranging from deep red (730 nm) to IR (1,000 nm) for a total duration of 10 ms. Consistent with the human results above, we observed robust photoreceptor responses at 1,000 nm (Fig. 3*A*, *Right*) comparable in waveform to these at 730 nm (Fig. 3*A*, *Left*). Plotting the amplitudes of these responses as a function of light energy revealed that the response amplitude increase as a function of light power was steeper at 1,000 nm. In this particular retina, Eq. **3** with $n = 1.4$ ($Q_{1/2} = 3.1 \times 10^7$ photons/μm$^2$) described the data well for 730-nm stimulation but a much higher $n = 2.4$ ($Q_{1/2} = 4.6 \times 10^8$ photons/μm$^2$) was needed to describe

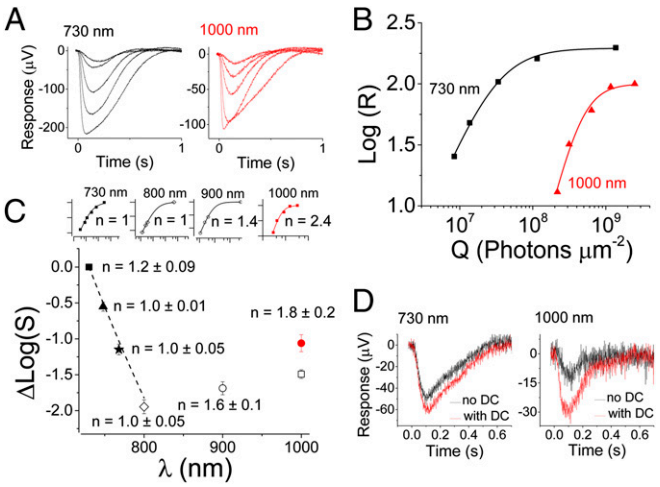


**Fig. 3.** WT mouse rods respond to IR light with much greater sensitivity than predicted by 1PO excitation theory. (*A*) Rod photoresponses to 10-ms stimulation with varying light energy at 730 (*Left*) and 1,000 nm (*Right*). (*B*) Amplitude data from responses in *A* are shown as a function of flash energy in photons per micrometer squared. Data were fitted with Eq. **2**, with $n = 1.4$ and $Q_{1/2} = 3.1 \times 10^7$ photons/μm$^2$ (730 nm) and with $n = 2.4$ and $Q_{1/2} = 4.6 \times 10^8$ photons/μm$^2$ (1,000 nm). (*C*) Average (four mice) rod sensitivity ($S = 1/Q_{1/2}$) normalized to the sensitivity at 730 nm (black square) plotted as a function of wavelength (λ) 748 nm (triangle), 768 nm (star), 800 nm (open diamond), 900 nm (open circle), and 1,000 nm (open square or red circle, see below). Small insets show the normalized logarithmic amplitude data from one representative retina [*x* scale 1 $\log_{10}(Q)$ and *y* scale 0.5 $\log(R/R_{max})$]. Eq. **2** was fitted to each dataset with $Q_{1/2}$ (730 nm) = $1.6 \times 10^8$ photons/μm$^2$ and $Q_{1/2}$ (800 nm) = $9.4 \times 10^9$ photons/μm$^2$. The response–energy function became steeper for 900- and 1,000-nm stimulation and could be described by an exponential factor $n > 1$ (*Methods*). Assuming the maximum amplitude to be the same as at 730 nm yielded $n = 1.4$ for this particular retina with $Q_{1/2}$ of $4.9 \times 10^9$ photons/μm$^2$ (900 nm) and $3.5 \times 10^9$ photons/μm$^2$ (1,000 nm, no inset). The average sensitivity for two retinas where saturation became evident (*A* and *B*) at 1,000 nm is shown as a red circle. This sensitivity is higher because the maximum amplitude at 1,000 nm was smaller than that at 730 nm. Setting the maximum in this way also yielded a steeper response–energy function as shown in the *Inset* and *B* (red). (*D*) Effect of pulsed laser light dispersion on rod sensitivity at 730 (*Left*) and 1,000 nm (*Right*). Black traces show responses to $6.6 \times 10^7$ photons/μm$^2$ (730 nm) and $1.6 \times 10^9$ photons/μm$^2$ (1,000 nm) flashes without dispersion compensation (DC). Red traces show the corresponding responses with DC, providing evidence that rod sensitivity is significantly affected by DC with 1,000-nm but not with 730-nm laser light stimulation.

the data obtained at 1,000 nm (Fig. 3*B*). The half-saturating stimulus energy at 730 nm was estimated to correspond to 29 rhodopsin isomerizations (R*) per rod, comparable to the known mouse rod sensitivity determined by using ∼500-nm light (23–25). We did not detect any evidence of progressive decline in the amplitude of the responses; however, saturating the response at 1,000 nm was not always possible, even with the maximum attainable light power. We believe that this was due to a combination of factors: (*i*) slight variations in the sensitivity of individual retinas (as a rule, retinas that showed highest sensitivity at 730 nm could also be saturated at 1,000 nm), (*ii*) we were already working with the maximal possible power at 1,000 nm, which did not allow us to increase flash strength further to always obtain saturated responses, and (*iii*) imperfect focusing of the laser beam onto the photoreceptor outer segment layer, which would affect 2PO activation at 1,000 nm but not 1PO at 730 nm (Fig. 3*D*). To avoid introducing bias in our analysis by this issue, we set the maximum amplitude for each wavelength to that attained with 730-nm stimulation to determine the $Q_{1/2}$ value at each wavelength. This approach allowed us to examine the spectral sensitivity relative to that obtained at 730 nm for each retina. The sensitivity declined according to a pigment template up to 800 nm (dashed line in Fig. 3*C*) (24). However, this trend reversed and the sensitivity increased on stimulation with 900- or 1,000-nm light. The sensitivity at 1,000 nm was 0.5 log-units higher than at 800 nm when the maximum response was assumed to be equal at all wavelengths. On average, the slope *n* of the response–flash energy data increased from 1.2 ± 0.09 at 730 nm to 1.8 ± 0.2 at 1,000 nm (six retinas). In some retinas, we obtained near-saturated responses and could directly measure the maximal response at 1,000 nm (Fig. 3 *A*, *Right*, *B*, and *C*, *Inset*). Interestingly, the maximum amplitude at 1,000 nm was ∼50% of that measured at 730 nm (Fig. 3*B*), suggesting that pigment isomerization at 1,000 nm was constrained to a fraction of the length of the photoreceptor outer segments. As a result, the relative sensitivity at 1,000 nm for retinas where saturation was evident at that wavelength (red circle in Fig. 3*C*) was only ∼1 log-unit lower compared with that at 730 nm. Also, our analysis might have underestimated the slope value *n* at 1,000 nm due to the assumption of identical maximal response amplitudes at 1,000 and 730 nm. Altogether, the approximately twofold steeper intensity–response curve at 1,000 nm compared with the one at 730 nm, the activation of just a fraction of the outer segments, and the distinct increase in relative sensitivity at wavelengths longer than 800 nm support phototransduction triggered by 2PO absorption. This conclusion is consistent with earlier results by Gray–Keller et al., suggesting that phototransduction can be activated by near IR light of rhodopsin in Gecko rods (13).

Because we stimulated dark-adapted retinas with short flashes that did not cause significant bleaching of visual pigments, responses like those shown in Fig. 3*A* were expected to be dominated by rod photoreceptors in mouse retina where 97% of total photoreceptors are rods, even in the central part of the retina. To confirm that the data shown in Fig. 3 were largely derived from rods, we recorded responses from *Gnat2*$^{-/-}$ mouse retinas wherein cones cannot produce light responses (26). No significant differences were observed between WT and *Gnat2*$^{-/-}$ retinas. We also recorded from *Gnat1*$^{-/-}$ mice with rods that cannot produce light responses (27) and from young *Rho*$^{-/-}$ mice (28) that have functional cones but lack rod visual pigment. Under the recording conditions used, cones were ∼2 log-units less sensitive than rods, and their maximum response amplitudes were ∼30 μV. Although the sensitivity and amplitudes of cone responses were smaller than those of rods, we did record small 1- to 3-μV responses from *Gnat1*$^{-/-}$ and *Rho*$^{-/-}$ retinas with the maximum laser light available at 1,000 nm (∼$2 \times 10^9$ photons/μm$^2$). Together, results from these mice with only cone-mediated vision suggest that retinas without functional rods or without any rod pigment can also respond to 1,000-nm light. Such minute cone-driven maximal responses are consistent with our results from *Gnat2*$^{-/-}$ mice and indicate that under normal conditions the cone contribution to the overall retina IR response is minor in mice.

As ultra-short femtosecond laser pulses were used for stimulation, we also tested how broadening of the laser pulses in the time domain, i.e., dispersion, affects the photoreceptor response to different wavelengths. Dispersion does not affect the average power and, therefore, the probability of a 1PO excitation of the visual pigment. However, broadening of the pulses decreases the probability of a 2PO absorption event (12). In the experiments described above, we minimized dispersion with our dispersion compensation system. Fig. 3*D* shows how the rod response was affected by turning the dispersion compensation off. As expected, amplitudes of responses to a 730-nm flash that produced ∼20% of the maximal response when light was compensated for dispersion (red trace) were only marginally smaller when the dispersion compensation was turned off (black trace). In contrast, on 1,000-nm stimulation, minimizing the dispersion of the laser light pulse increased the response by 2.5-fold (Fig. 3*D*, *Right*), indicating that the rod light response was produced by a nonlinear optical process. We also measured the 2PO excited spectra from isolated mouse retinas, and even though we could measure fluorescence emission from rod cells with 1,000-nm excitation, we could not detect any appreciable SHG signal (Fig. S1). At 730-nm excitation, maximal emission was at 480 nm, consistent with the fluorescence of all-*trans*-retinol present in rod outer segments (ROSs). The reduced fluorescence in response to 1,000-nm excitation is produced by rhodopsin with a minor contribution from other fluorophores present in ROS. These data indicate that rod responses to near IR light were generated by a 2PO absorption process rather than SHG.

**Visual Pigment Activation by IR Light.** Biochemical studies were used to investigate the mechanisms producing visual sensations in humans and electrophysiological signals in mice in response to IR illumination. First, we investigated whether rhodopsin (structure shown in Fig. 4*A*, *Left*) and cone pigments could be activated by absorption of IR light. Absorbance spectra of detergent-solubilized rhodopsin were compared before and after exposure to 1,000-nm ($2 \times \lambda_{max}$ of rhodopsin) laser light. As expected, the absorbance maximum for rhodopsin was at 500 nm in the dark, reflecting the ground state of rhodopsin. Exposure to 1,000-nm laser light shifted the absorbance peak to ∼380 nm (Fig. 4*A*, *Center*), producing a spectrum similar to the one observed on bleaching rhodopsin with visible light (Fig. S2). To determine whether rhodopsin had undergone denaturation during this exposure to 1,000-nm light, the exposed sample was incubated with an excess of 11-*cis*-retinal overnight. This procedure regenerated the absorbance at 500 nm (ground state of rhodopsin; Fig. 4*A*, *Right*), indicating a lack of protein degradation.

Bleaching experiments also were performed with purified green and blue cone pigments. Similar to the result with rhodopsin, we found that the absorbance maximum of green cone pigment (regenerated with 9-*cis*-retinal) shifted on exposure to 1,000-nm light from 496 to ∼380 nm. Moreover, this shift also was largely reversed by treatment with 9-*cis*-retinal (Fig. S3*A*). In the case of 11-*cis*-retinal–bound blue cone pigment, bleaching with 850-nm light shifted the absorbance maximum from ∼415 to ∼380 nm (Fig. S3*B*).

In our experimental setup, it was difficult to scan the entire sample with a focused IR laser beam that resulted in less than 100% bleaching. In the first experiment, ∼20% of rhodopsin remained in the ground state. More than 95% of the photoactivated rhodopsin was reconstituted into ground-state rhodopsin on overnight incubation with 11-*cis*-retinal. With the green cone pigment, 67% of the sample was bleached with the IR laser, and of this, 70% was reconstituted back to the ground state on

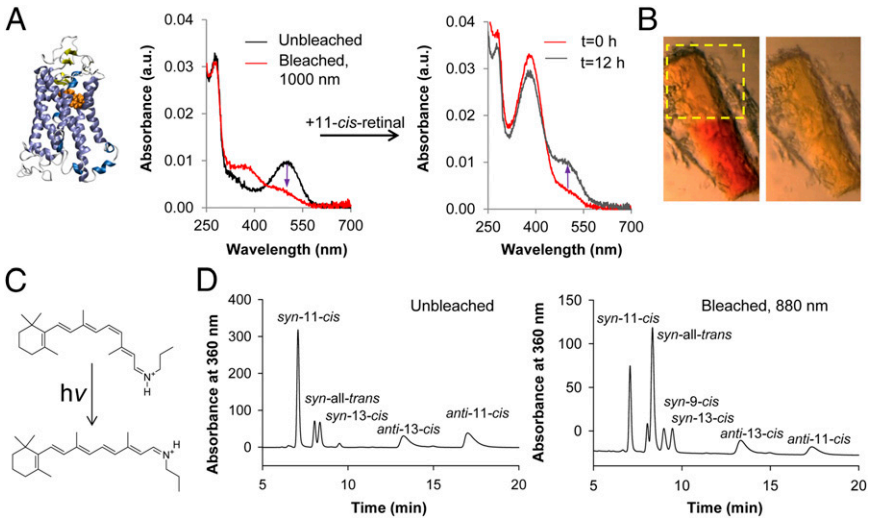


**Fig. 4.** IR isomerization of native and model visual pigments. (*A*) Bleaching of detergent-solubilized bovine rhodopsin with 1,000-nm light. (*Left*) Structure of rhodopsin is shown. (*Center*) Absorption spectra from detergent-solibilized bovine rhodopsin are presented. The spectrum from the control unbleached sample is shown in black and the spectrum after bleaching with 1,000-nm laser light is in red; the indigo arrow indicates the loss in 500-nm absorbance. (*Right*) Absorption spectra are shown immediately after adding an excess of 11-*cis*-retinal (red) and after overnight incubation on ice (black). The indigo arrow indicates the recovery of 500-nm absorbance. (*B*) Bleaching of a rhodopsin crystal with 1,000-nm light. (*Left*) Image obtained with visible light by using a sectioning microscope immediately after IR bleaching. The yellow rectangle outlines the region that was bleached with 1,000-nm light and the red color of the unbleached lower portion of the crystal is clearly visible. (*Right*) Picture obtained after bleaching the entire crystal with white light. (*C*) Chemical formulas of the protonated Schiff base. (*Upper*) 11-*cis*-propylamine Schiff base. (*Lower*) All-*trans*-propylamine Schiff base. (*D*) The protonated 11-*cis*-retinal-propylamine Schiff base was isomerized by intense IR light at 880 nm. Shown are HPLC chromatograms of Schiff bases after conversion into their oximes. (*Left*) Unbleached control. (*Right*) Sample bleached with 880-nm light. Isomers indicated in each chromatogram are as follows: 11-*cis,* 11-*cis*-retinal oxime; 13-*cis*, 13-*cis*-retinal oxime; 9-*cis,* 9-*cis*-retinal oxime; all-*trans,* all-*trans*-retinal oxime.

incubation with 9-*cis*-retinal. About 50% of the blue cone pigment sample was bleached with the IR laser. However, neither the IR-bleached nor white light-bleached blue-cone pigment samples were reconstituted by overnight incubation with 11-*cis*-retinal. The reason for failing to fully reconstitute the cone opsins with free 9-*cis*- or 11-*cis*-retinal is unclear, but this observation is consistent with studies showing that the dynamics of 11-*cis*- and all-*trans*-retinal in the binding pockets of cone pigments differ from those of rhodopsin (29–31).

To test further whether visual pigment can be activated directly by IR light, we exposed part of a rhodopsin crystal to 1,000-nm light and found that it changed color from red to yellow (Fig. 4*B*, *Left*) (32). As expected, control illumination of the entire crystal with white light turned the rest of the crystal yellow as well (Fig. 4*B*, *Right*). Finally, we measured the 2PO excited emission spectra from a bleached rhodopsin crystal that was exposed to both 1,000 nm and white light by using an excitation laser light in the range of 740–1,000 nm (Fig. S4). The resulting spectra did not contain any SHG signature and were found to be consistent with spectra from photo-activated rhodopsin previously published for 1PO and 2PO excitation (15, 33). Thus, these biochemical experiments rule out SHG from visual pigments either in a crystal or solution as the cause of visual pigment activation by IR light.

**Chromophore Isomerization by IR Light.** We next investigated if IR light could directly isomerize a model visual chromophore, namely the protonated 11-*cis*-retinyl-propylamine Schiff base (Fig. 4*C*). Light-exposed and unexposed protonated retinylidene-propylamine Schiff base samples were analyzed by normal-phase HPLC (34). The dominant 880-nm light isomerization product was all-*trans*, with trace amounts of 9-*cis* and 13-*cis* retinoids (Fig. 4*D*). This distribution of retinoid isomers was similar to that obtained with visible light-catalyzed photoisomerization of either the 11-*cis*-retinylidene Schiff base (Fig. S5) or all-*trans* retinal (35). The sample treated with IR light at 880 nm for 2 h retained only 20% of the original 11-*cis*-retinoids (Fig. 4*D*, *Right*), whereas under dark conditions, at least 70% of the 11-*cis*-retinoids remained (Fig. 4*D*, *Left* and Fig. S5). This result implies that the 11-*cis*-retinoids were photoisomerized with IR light of about twice the wavelength of the maximal absorbance of the protonated 11-*cis*-retinylidene Schiff base (435 nm).

Taken together, these data demonstrate that IR light from a femtosecond laser can directly activate rod and cone visual pigments and trigger the isomerization of visual chromophore. Additionally, as no SHG signal was observed in the rhodopsin spectra from either crystals or solution (15) even when stimulating IR light with double the wavelength of rhodopsin's maximal absorbance was used, the data further suggest that activation of visual pigments and isomerization of visual chromophore are initiated by a 2PO absorption process.

**Molecular Modeling Studies.** Next, we performed hybrid quantum-mechanical calculations coupled to molecular dynamics simulations (QM/MM) to examine the energetics of 2PO activation of rhodopsin (Fig. S6). Fig. 5 reveals the predicted cross section for 2PO absorption from a monochromatic light source by rhodopsin obtained by using quadratic response time-dependent density functional theory (36). Calculations predicted nonnegligible values for the 2PO cross section between 950 and 1,150 nm, with a maximum peak at ~1,000 nm. The positions of the computed cross sections matched well with experimental data showing the increased sensitivity of IR radiation in mouse retinal electrophysiology (Fig. 3*C*). Absorption of two photons in this wavelength range results in electronic excitation of the rhodopsin chromophore into its first excited state. This well-characterized state (37–39) corresponds to the $\pi\pi^*$ transition responsible for the rapid *cis-trans* retinal isomerization that initiates phototransduction.

## Discussion

Results obtained from human psychophysics presented in Fig. 1*B* showed that humans can detect IR light from laser beams. The

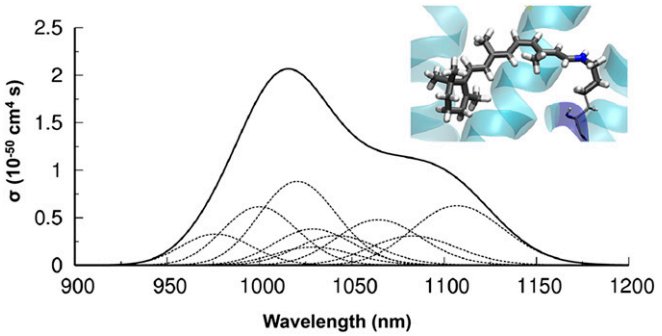


**Fig. 5.** Rhodopsin 2PO cross sections from hybrid QM/MM calculations. Computed 2PO cross section from quadratic response and TD-DFT at the CAM-B3LYP(66) level of theory (36). The thin dashed lines represent contributions from single thermally equilibrated configurations sampled during QM/MM dynamics. (*Inset*) QM region defined in the calculations (represented in thick licorice), comprising the protonated Schiff base formed by condensation of 11-*cis*-retinal with the Lys296 side-chain.

analysis of results from 30 volunteers matching perceptions caused by the IR beam and visible light revealed that the perceived wavelength was slightly longer than half of the stimulating IR wavelength. The largest spread of results and most pronounced deviations from frequency-doubled points were observed for 1,000–1,100 nm. The cause of the slight red shift is not clear and probably has many sources. Although cone pigments are responsible for color perception, lack of their crystal structures prevented us from calculating their 2PO absorption spectra, but these may not exactly match the corresponding half-wavelength 1PO spectra. Additionally, emission of photons caused by 2PO absorption in rhodopsin is possible (Fig. S1) (33). Excitation of rod cells with a 1,000-nm light caused emission with maximum at ∼560 nm. This additional weak radiation could potentially explain both effects observed in our experiments with color matching in humans, namely the red shift (Fig. 1*B*) and increased SD for 1,020- and 1,040-nm IR stimuli.

Single-photon events can clearly be induced with 850-nm light as optical coherent tomography (OCT) scanning with this wavelength causes the human perception of red light (40). Our data at low laser powers indicate that 1PO excitation is still dominant for wavelengths shorter than 900 nm even for ultrashort IR pulses (Fig. 2). This region of wavelengths is in good agreement with Wald and colleague's results (7), even though different sources of light and methodologies were used in these experiments. In our spectral sensitivity experiments, we varied the pulse duration. Using excitation around 1,000 nm, the minimum laser power needed to evoke perception of light was more than 100 times larger for long pulses than that needed for short pulses. This 100-fold increase along with perception of IR as light with colors corresponding to roughly half of the excitation wavelength indicated clearly isomerization via a nonlinear process. Whether the 2PO process might have contributed to Wald and colleagues's 1947 results cannot be excluded.

Results of our recordings from mouse retina are consistent with those of the human experiments and demonstrate that photoreceptors can be directly activated by IR light. The sharp deviation from the rhodopsin one-photon spectral template (Fig. 3*C*) and actual increase in spectral sensitivity at long wavelengths (900–1,000 nm) indicate that activation of rhodopsin with IR light is not caused by a linear 1PO process but rather by a nonlinear optical process. This nonlinearity was confirmed by an increased slope of the mouse rod intensity–response curve at 1000 nm compared with shorter wavelengths (Fig. 3*B*). A nonlinearity of the response to IR light was previously reported in lizard photoreceptors (13). Also consistent with this notion is that the maximal response at 1,000 nm in our experiments was smaller than that at 730 nm (Fig. 3*B*), which indicates activation of phototransduction in only a portion/section of ROS. The larger effect of dispersion compensation at 1,000 nm compared with 730 nm (Fig. 3*D*) also indicates 2PO activation as the mechanism of rhodopsin activation by IR light. Our recordings from mouse retina show that the shift from 1PO to 2PO activation occurs between 800 and 900 nm (Fig. 3*C*), consistent with our human results above. As the mouse photoreceptors were directly illuminated in these experiments, SHG from the cornea and lens can be ruled out. Additionally, there was no SHG signature in the spectra from mouse retina. Together, these two findings indicate that the most likely mechanism responsible for visual pigment activation by IR is 2PO absorption.

To test further the hypothesis that 2PO excitation of rhodopsin dominates mouse rod responses at 1,000 nm, we compared the expected number of 2PO rhodopsin isomerizations at 1,000 nm estimated from our QM/MM simulations with the 1PO isomerizations at 730 nm. We calculated the number of activated rhodopsin (R*) molecules per rod (Φ) to be equal to 101, using the number of photons per micrometer squared calculated from Eq. **2** and using collecting area of the rod $a_c$ (730 nm) = $9.3 \times 10^{-7}$ μm$^2$ calculated per Heikkinen et al. (23). This value falls within the range of previously published sensitivities for mammalian rods (see ref. 23, with 77 R* or ref. 25 with 20 R*). If attenuation of the 0.5-mm polycarbonate layer and 0.2-mm perfusion solution layer above the retina is factored in, the value of Φ declines to ∼90 R* per rod. To estimate rhodopsin isomerizations by 2PO absorption of 1,000-nm light, we calculated the number of 2PO absorption events per molecule per pulse based on Denk et al. (12) to be equal to $4.88 \times 10^{-7}$, by using a cross section for 2PO absorption from our QM/MM simulations and setting the numerical aperture of the focusing objective as 0.125 to account for spreading of the laser beam caused by the specimen holder's polycarbonate layer and uncertainty about the alignment between the focal volume of the laser spot and the outer segment layer of the retina. Then using a quantum yield for isomerization equal to 0.6 (assuming that 1PO and 2PO quantum yields are the same after scaling the wavelengths by 1/2) (41), a ground-state rhodopsin concentration of 5 mM, and approximately six pulses per rod cell, we found that the 10-ms stimulation by the half-saturating power of 6 mW (Fig. 3 *B* and *C*, red point) corresponds to 166 excited rhodopsin molecules per rod. This number, although still an overestimate due to pulse spreading in the time domain introduced by the sample setup, is in agreement with the sensitivity of rods under our recording conditions and supports the conclusion that a direct 2PO excitation of rhodopsin molecules triggers mouse rod responses at 1,000 nm.

Agreement between the experimental mouse electrophysiology results and calculations based on direct isomerization by 2PO absorption favors a direct photoisomerization over a two-step process such as photoisomerization of rhodopsin by 2PO-induced rhodopsin fluorescence, as the dominant mechanism. Assuming that rhodopsin 2PO absorption cross sections are the same for 2PO isomerization and 2PO fluorescence and using a rhodopsin photoisomerization quantum yield of 0.6 and a fluorescence quantum yield of $0.9 \times 10^{-5}$ (15), we estimate the rod electrophysiological responses would have been 70,000-fold smaller even if every fluorescent photon was absorbed by a rhodopsin molecule and resulted in photoisomerization (quantum yield, 0.6). There are other fluorescent molecules in the ROS, such as all-*trans*-retinol and NADPH. However, their excitation with a 1,000-nm beam would require three-photon absorption, which not only disagrees with the electrophysiological data, but also would occur with absorption cross sections $10^{33}$ times smaller than those of 2PO in general (20, 42).

Human psychophysical data and our mouse cone recordings indicate that cones can respond to IR light via a nonlinear process. To test the feasibility of 2PO absorption-triggered

cone-mediated visual sensation, we estimated the number of cone pigment isomerizations in our human experiments. We set the 2PO cross section of the cone pigment to the same value as that for rhodopsin. Using conditions of the human scanning experiment, i.e., a 20-μm spot on the retina, a scanning speed of 10 Hz, a pulse repetition frequency at 76 MHz, and a pulse duration of 200 fs, we calculated as noted for mice above, the number of 2PO absorption events per molecule of cone pigment per pulse to be equal to $1.8 \times 10^{-11}$. Assuming a ground-state cone pigment concentration of 3 mM, we found that 1,000-nm pulsed laser light at 1-mW average power should produce an average of 27 activated cone pigment molecules during one scan line per cone in the foveal area. Even though this estimate does not account for dispersion, it is above recent estimates for the psychophysical cone vision threshold (43), suggesting that direct 2PO isomerization of cone pigments is a plausible mechanism for human cone-mediated IR perception.

Here, biochemical studies further indicate that 2PO-induced isomerization of visual pigments and the model chromophore is a safe, reversible process that produces the same reaction products as white light, 1PO-induced isomerization. Ground states of rhodopsin and green cone pigment were restored after bleaching and subsequent incubation with 11-*cis*- or 9-*cis*-retinal. The color change of a rhodopsin crystal on irradiation with 1,000-nm light or with white light was the same. Illumination of a model visual chromophore, a protonated 11-*cis*-retinyl-propylamine Schiff base, with IR light produced a nearly identical distribution of retinoid isomers to that caused by photoisomerization with visible light. Thus, a 1PO or 2PO event most likely results in the same isomerization process, producing all-*trans*-retinal that is recycled back to the active *cis* chromophore through the visual cycle (44).

Our human and mouse results were further supported by QM/MM modeling. Our calculations predicted an efficient absorption of radiation in the IR range by a 2PO absorption mechanism at frequencies centered around 1000–1,100 nm. These data are in agreement with our psychophysical and electrophysiological data, strongly supporting the assertion that 2PO absorption at these wavelengths indeed caused isomerization. 2PO absorption at ∼1,000 nm produced a population featuring the first $\pi\pi^*$ electronic excited state of retinal. This outcome means that nearly simultaneous absorption of two low-energy photons results in the same excited state that triggers the fast *cis-trans* 1PO isomerization of retinal that drives visual perception. Bleaching of rod and cone pigments by IR irradiation (Fig. 4 and Fig. S3) supports this notion and also indicates that the IR light-bleached pigment can be regenerated through the visual cycle (44).

The evidence derived from this study suggests a dominant role for 2PO absorption and isomerization. Rhodopsin can spontaneously be activated by heat (4), and local heating by the train of IR photons could add to probability of isomerization by 1PO as demonstrated theoretically (45). However, the effects of dispersion and quadratic dependence of responses versus laser power would not be so clearly observed. Considering energetics of photoisomerization and thermal isomerization (45), we expect that, at the same photon intensity, the probability of thermally assisted isomerization would decay with lowering the energy, namely increasing the wavelength of the impinging IR photons. In the case of nonresonant 1PO excitation facilitated by vibrational heating of the sample, the thermal vibrational excitation of the ground state decreases as the impinging photons become less energetic. At the same time, the energy of the optically exciting photon decreases as well, thus reducing the global probability of a 1PO excitation from a vibrationally thermally excited ground state. In contrast, our data in both human and rodent experiments clearly show an increase in spectral sensitivity with a decrease in impinging photon energy in the IR range, thereby indicating that a thermal contribution does not play a major role in perceiving IR as visible light with colors corresponding to roughly 1/2 wavelength of the excitation light. Collectively, our data including human psychophysics, mouse electrophysiology, biochemical experiments, and quantum-mechanical calculations provide a supportive foundation that 2PO isomerization is most likely the predominant mechanism.

In summary, although the human eye structure and the absorption spectra of pigments that produce isomerization of the 11-*cis*-retinylidene chromophore limit our visual perception of light, and in consequence our visual perception is most responsive to stimulating light in the 400- to 720-nm (visible) range, our results demonstrate that humans can also detect IR light seen as visual light that clearly arises from 2PO absorption and direct isomerization of the retinoid chromophore rather than from a SHG process. QM/MM modeling and experimental data with purified compounds indicate that 2PO absorption at ∼1,000 nm produces a population of the first $\pi\pi^*$ electronic excited state of retinal, the state well characterized previously for a 1PO isomerization. First a virtual state is formed by interaction with the first photon, followed by relaxation of the virtual state before absorption of the second photon pushes the system into an excited state that causes isomerization. Considering that only 1 mW of IR beam power was needed to create visual sensation in humans, this discovery could have implications for developing technologies that use this phenomenon. IR excitation could also be used for deep tissue penetration expressing a variety of optogenetic probes.

## Methods

**Human Psychophysics.** Visual perception caused by IR light in the human eye was investigated in vivo. All tests were conducted in compliance with American National Standard Institute (ANSI Z136.1) and European Standards (EN 60825–1) providing recommendations for permissible exposure limits of laser light. We also implemented safety procedures described in the literature (46) for ophthalmic devices, especially scanning laser ophthalmoscopes and fundus autofluorescence devices. The study was approved by the Ethics Committee of the Collegium Medicum in Bydgoszcz, Nicolaus Copernicus University in Torun, Poland. Examinations were carried out only after written informed consent was obtained.

The human psychophysics experiments were performed under dark room conditions. At the level of the subject's eye, the average luminance was 0.6 lx. The optical setup was isolated from residual ambient light by its dedicated housing. In the optical setup, we included a cutoff filter (Chroma T750lpxxr) to ensure that there was no leakage of the pump laser frequency. During spectral sensitivity experiments, a subject's head was covered by a black curtain attached to the housing. Before sensitivity testing, all human subjects were dark adapted in low light (0.6 lx) conditions for 2 h and then for another 20 min under this black curtain.

Color matching experiments were performed to determine an individual's perception of color associated with a given frequency-doubled wavelength during scanning of his/her retina by an IR femtosecond laser beam.

The test was performed on the left eyes of 30 healthy volunteers aged 21–38 y, both males and females. We constructed a simple experimental optical setup that included modifications derived from earlier experiments (8, 9). Dmitriev and colleagues had used 20-ns pulses and localized constant patterns projected onto the retina (10). Here we used 200-fs (76-MHz repetition rate) laser light pulses ranging from 950 to 1,200 nm generated by an optical parametric amplifier (OPO) (Emerald; APE), except for a 1,040-nm light originating directly from the laser pumping OPO (Femtotrain; HighQLasers). Estimated length of pulses at the cornea was in the picosecond range due to dispersive broadening in the fibers and optical setup. Instead of projecting large patterns, we focused the beam onto a 20-μm spot in the retina.

Beam power measured on the cornea was equal to 1 mW for beams spanning 950–1,125 nm and 1.5 mW for those covering 1,150 and 1200 nm, well below ANSI and EU standards for maximum permissible power (MPΦ) (American National Standard for Safe use of Lasers; ANSI Z136.1-2007). Calculations of MPΦ were performed using a stationary beam. The single pulse model at 950 nm yielded 1.39 W (at 1,100 nm, 4.39 W; at 1,200 nm, 34.9 W). The average power heat buildup model at 950 nm gave a MPΦ of 1.21 mW, and at 1,100 and 1,200 nm were 1.93 and 153 mW, respectively (46). To provide an increased safety margin, we added a beam scanning system that provided full control over the intensity of optical radiation power delivered to the eye as a function of time.

The laser beam was directed to the retina by a pair of IR galvoscanners that created a single linear scan on the fundus perceived by the volunteer as a single horizontal line. In close proximity to this line, we projected a similar-shaped horizontal line of visible radiation originating from a halogen lamp and transmitted through a monochromator (spectral width of 8 nm). Volunteers then were asked to match the colors of the two lines by manually adjusting the wavelength of the second line projected onto the retina via the monochromator. The wavelength of the beam from the monochromator was measured independently by a spectrometer. A schematic for this setup is shown in Fig. 1*A*. A 20-μm scanning beam enabled the extraction of many photoreceptors simultaneously. For example, 15–60 cones were excited by the beam as a function of retinal location.

Our optical methodology was a modification of that presented by Dmitriev et al. (9). However, compared with these early studies, measurement points in our study did not fall on the double-frequency line. The explanation may involve a significant difference in the quality of the experimental setup. We used a focused beam of well-controlled optical exposure with much shorter pulses providing a five order of magnitude difference in the initial pulse length. (Taking into account pulse stretching caused by dispersive elements in the optical setup and the human eye, this pulse was still at least 10,000 times shorter in our experiments.) With these experimental settings, it was very easy to see the signal generated by IR radiation, even in ambient light. A high repetition rate of the laser ensured that we should be far from the frequency range responsible for color illusions, which are usually in the range of hundreds of hertz.

Measurements of spectral sensitivity (Fig. 2) were made with a modified experimental optical setup compared with the one shown in Fig. 1. Modifications were as follows: (*i*) the reference arm, including the monochromator (AM) and a spectrometer, was blocked; (*ii*) the dichroic mirror was replaced by a beam-splitter to divide the beam and direct a defined portion of the beam (~33%) onto the laser power meter connected to a personal computer (PC); (*iii*) to obtain long pulses, the laser beam was routed through 1 km of a fiber spool (Corning HI780); and (*iv*) an adjustable neutral gradient filter was placed at the output of the laser. To measure minimal power of the laser beam that still caused a visual sensation, this filter was adjusted by the subject during the test procedure. After careful calibration, the optical power recorded by the PC corresponded to the optical power of the IR beam reaching the cornea. Values measured by the power meter were saved in PC memory after the tested subject pressed a mouse button. Both tested subjects were healthy volunteers: S1, a 37-y-old woman; S2, a 34-y-old man.

To achieve the best viewing comfort for a subject, the laser beam illuminating the retina also scanned along a horizontal line. The edges of this line (corresponding to scanner turnout points) were blocked by a diaphragm placed in the focal plane of the first lens after the scanners. Measurements were repeated 12 times (on further analysis, 10 values were used after rejection of 2 extreme values). Then the wavelength of the OPO light source was changed into the next one. Measurements started from short wavelengths to long. If a subject needed to "take a break" during testing, the tested eye was covered by a black patch before he/she emerged from under the black curtain back into dark room conditions.

Measurements with both short and stretched pulses were performed within 2 d. Repeatable localization of the beam on the retina was assured by fixation of the chinrest with respect to the objective. Additionally, the central position and length of the projected pattern (line) also served to achieve fixation: the entire line was projected onto the retina only when the scanning pivot point was in the central position of the eye pupil. Both long and short pulses were affected by the dispersion of the optical system. Elongation of pulses in the time domain was estimated assuming a Gaussian pulse and using Eq. **1** (47)

$$\tau_{out} = \tau_{in} + \left[1 + 7.68 * \frac{(D * L)^2}{\tau_{in}^4}\right]^{\frac{1}{2}}. \quad [1]$$

In this equation, $D$ stands for the dispersion, $L$ for the optical path length, $\tau_{in}$ is the duration of the input pulse, and $\tau_{out}$ is the duration of the elongated pulse. We calculated that, by the time 200-fs laser pulses reached the cornea, they were elongated to 1.25 ps at 800 nm and to 0.5 ps at 1,150 nm. Longer pulses, obtained by dispersive stretching of the pulse through the fiber spool, were calculated by assuming known dispersion characteristics of the fiber. At the cornea, their durations varied from 0.6 ns at 800 nm to 0.3 ns at 1,060 nm.

**Mice.** All animal procedures and experiments were approved by the Institutional Animal Care and Use Committee at Case Western Reserve University and conformed to recommendations of both the American Veterinary Medical Association Panel on Euthanasia and the Association for Research in Vision and Ophthalmology. C57BL//6J mice were purchased from the Jackson Laboratory. *Gnat2*$^{-/-}$ mice [*Gnat2*$^{cpfl3/cpfl3}$ (26); B6.Cg-*Gnat2*$^{cpfl3}$/Boc, stock number 6795] also were also obtained from the Jackson Laboratory. *Gnat1*$^{-/-}$ and *Rho*$^{-/-}$ mice were kindly provided by Janis Lem (Tufts University, Boston) and genotyped as previously noted (27, 48). All mice were housed in the animal facility at the School of Medicine, Case Western Reserve University, where they were provided with a regular mouse chow diet and maintained either under complete darkness or in a 12-h light (~10 lx)/12-h dark cyclic environment. Euthanasia was performed in compliance with American Veterinary Medical Association Guidelines on Euthanasia and with approval by the Case Western Reserve University Institutional Animal Care and Use Committee. All mice used in this study were of mixed sex and between 1 and 3 mo old.

**Mouse Electrophysiology.** Transretinal ERGs recorded from isolated retinas of WT (C57BL/6J) and cone transducin knockout (*Gnat2*$^{-/-}$) mice between 1 and 2 mo old were used to study rod photoreceptor responses to 730- to 1,000-nm light stimuli. Rod transducin KO (*Gnat1*$^{-/-}$) and young 1-mo-old rhodopsin KO (*Rho*$^{-/-}$) mice were used to determine the cone component of the light response. Dark-adapted (>12 h) animals were euthanized, their eyes were enucleated and bisected along the equator, and their retinas were detached under dim red light. Each retina was mounted photoreceptor side up on filter paper attached to a custom-built specimen holder similar to that described in figure 1 of Nymark et al. (49). The retina was perfused at 3–5 mL/min with Ringer solution containing the following (mM): $Na^+$, 133.9; $K^+$, 3.3; $Mg^{2+}$, 2.0; $Ca^{2+}$, 1.0; $Cl^-$, 143.2; glucose, 10.0; EDTA, 0.01; Hepes, 12.0; and 0.72 g/L Leibovitz culture medium L-15 buffered to pH 7.5 with NaOH. DL-AP4 (40 μM) and $BaCl_2$ (100 μM) were used to isolate the photoreceptor component of the ERG signal. All chemicals except DL-AP4 (Tocris) were purchased from Sigma-Aldrich. The heating unit, amplifier, and software of the commercial in vivo ERG system (LKC Technologies) were used to collect transretinal ERG responses at 37 °C. Data were sampled at 1 kHz and low-pass filtered at 300 Hz (8-pole Bessel). The specimen holder was aligned under the 2PO microscope (TCS SP5; Leica) used to deliver pulsed laser light stimuli (80 MHz, 75 fs) tuned between 730 and 1,020 nm (Chameleon Vision-S; Coherent). Pulse duration at the retina was affected by the dispersion properties of the optical system. We estimated that the pulse duration without dispersion compensation was four times longer than the one with dispersion compensation. The estimate was made by measuring changes in two-photon fluorescence from mouse retinal pigment epithelium, evoked with 1,000-nm light with and without dispersion compensation. Light was focused through a 0.25-NA objective (HCX FL PLAN, 10×/0.25; Leica) and scanned for 10 ms over a square 0.821 × 0.821-mm area (128 × 128 pixels) of the central retina. Laser power at the sample plane that was adjusted with microscope software was measured for each wavelength with a calibrated light meter (FieldMax-TO laser power meter; Coherent). We estimated the number of photons per micrometer squared produced by this stimulation by applying

$$Q = \frac{P\Delta t}{E_{photon}(\lambda)} \frac{1}{A}, \quad [2]$$

where $\Delta t$ (=10 ms) is the length of stimulus, $P$ is the average power of the laser measured at the level of the retina, $E_{photon}(\lambda)$ is the energy of a photon with wavelength $\lambda$, and $A$ is the full scanned area of the retina for the field of 821 × 821 μm.

The response amplitude ($R$) was fitted with a modified Naka–Rushton function (50) with exponential factor $n$ as follows:

$$\frac{R}{R_{max}} = \frac{Q^n}{Q^n + Q_{1/2}^n}, \quad [3]$$

where Q is the stimulus energy of the 10-ms light pulse (see above), $Q_{1/2}$ is the half-saturating stimulus energy, and $R_{max}$ is the amplitude of the saturated response. Because it was not always possible to saturate the photoresponse at longer wavelengths, we assumed that $R_{max}$ was similar across different wavelengths. As reviewed in *Results and Discussion*, this might not be the case if pigment isomerizations at 1,000 nm compared with 730-nm stimulation are restricted to a smaller volume within ROS. Sensitivity $S$ is defined as the reciprocal of $Q_{1/2}$ ($1/Q_{1/2}$).

**Computational Methods.**

***Initial setup.*** The structure of dark-state bovine rhodopsin from the Protein Data Bank (PDB ID code 1F88) (51) was used to start simulations. Hydrogen atoms were added to fill the valence, using protonation states for titrable

amino acids according to ref. (52). The protein was embedded in a pre-equilibrated 1-palmitoyl-2-oleoyl-sn-glycero-3-phosphoethanolamine (POPE) bilayer mimicking a natural membrane. The whole system was solvated by water with $Na^+$ counter-ions added to neutralize its total charge. The Amber force field (53) was used for the protein, and the generalized Amber force field (54) was used to determine force parameters for the retinal protonated Schiff base and palmitoyl lipids covalently bound to the protein. Parameters for POPE followed those from ref. (55). The TIP3P model was used for water (56). The system underwent 50 ns of classical MD simulations at constant pressure and temperature (1 atm, 300 K) for relaxation, using Langevin pistons and the SHAKE algorithm to constrain bonds containing H atoms (56). MD runs were done with the NAMD package (www.ks.uiuc.edu/Research/namd).

***QM/MM simulations.*** The protocol used here was similar to that published previously (57).

The system was partitioned into (*i*) a QM region, described at the density functional theory (DFT) level as in refs. 58 and 59, comprising the retinal Schiff base and the side-chain of the covalently bound Lys residue starting from its Cγ; and (*ii*) an MM region, comprising the remainder treated as above. The interaction between the classical and quantum parts was described by a fully Hamiltonian hierarchical coupling scheme (60, 61).

The whole system was allowed to evolve in time in the NVT (where N stands for fixed number of particles, V for fixed volume, and T for fixed temperature) ensemble, using the Nose–Hoover chain of thermostats (62–64). The Car–Parrinello Lagrangian scheme was used to model the time evolution of the quantum part (65), using a fictitious mass of 800 au for the electrons and a time step of 0.1209 fs. The system was simulated for a total of 15 ps. All QM/MM simulations were run with the CPMD code (www.cpmd.org).

***QM/MM 2PO excitation.*** 2PO excitation energies and cross sections were calculated within the QM/MM TD-DFT quadratic response framework (36) as implemented in the DALTON code using the CAM-B3LYP (66) xc functional and expanding the electronic density over the 6–311+G* basis set. This setup was reliably used to predict the 2PO excitation properties in archetypical channel rhodopsin (67). Transitions were computed over 10 structures sampled every 0.5 ps during the last 5 ps of the QM/MM MD run. The influence of the classically treated environment on the electronic properties of the QM region was taken into account by explicitly considering electrostatic coupling between the QM region and the classical restrained electrostatic potential (RESP) charges of residues with at least one atom as close as 5 Å to the QM part.

The position of the band was strongly influenced by both the instantaneous thermal deformation of the chromophore and the neighboring residues. In fact, the predicted scattering wavelengths for each single structure sampled during QM/MM simulations at a temperature of 300 K can differ by more than 100 nm. This outcome agrees with the results of 1PO excitation calculations for the same system, where the position of the absorption band is strongly dependent on the instantaneous thermal deformation of the protein and chromophore structures (68). It should be noted that our calculations refer to the ideal vertical transition, where concomitant absorption of the two photons takes place, and thus no structural relaxation on the virtual state occurs. The good match between our predictions and the experimental data is consistent with this notion indicating negligible relaxation.

Biochemical methods are provided in *SI Methods*.

**ACKNOWLEDGMENTS.** We thank Dr. L. T. Webster Jr. [Case Western Reserve University (CWRU)] and members of the K.P. laboratory for helpful comments on this manuscript. We thank Iwona Gorczynska for interesting discussions and Bartosz Sikorski, MD, for his medical advice. We thank W. Sun (Polgenix, Inc.) for expression of cone pigments and Z. Dong (Polgenix, Inc.) for preparation of mice and technical support. This work was supported by funding from National Eye Institute Grants R24EY021126 (to K.P.), R01EY009339 (to K.P.), R01EY019312 (to V.J.K.), R24EY021126 (to V.J.K.), P30EY002687 (to the Department of Ophthalmology and Visual Sciences at Washington University), and P30EY011373 (to CWRU); National Institute on Aging Grant R44AG043645 (to G.P.); and Research to Prevent Blindness. M.C. is supported by the Norwegian Research Council through Centre of Excellence Centre for Theoretical and Computational Chemistry Grants 179568/V30 and 171185/V30. M.W., K.K., and P.S. acknowledge the TEAM project financed by European Union within the framework of Innovative Economy coordinated by the Foundation for Polish Science. K.P. is John H. Hord Professor of Pharmacology.

1. Rodieck RW (1998) *The First Steps in Seeing* (Sinauer Associates, Sunderland, MA), p xi.
2. Crawford BH (1949) The scotopic visibility function. *Proc Phys Soc B* 62(5):321–334.
3. Kraft TW, Schneeweis DM, Schnapf JL (1993) Visual transduction in human rod photoreceptors. *J Physiol* 464:747–765.
4. St George RC (1952) The interplay o light and heat in bleaching rhodopsin. *J Gen Physiol* 35(3):495–517.
5. Luo DG, Yue WW, Ala-Laurila P, Yau KW (2011) Activation of visual pigments by light and heat. *Science* 332(6035):1307–1312.
6. Griffin DR, Hubbard R, Wald G (1947) The sensitivity of the human eye to infra-red radiation. *J Opt Soc Am* 37(7):546–554.
7. Lewis PR (1955) A theoretical interpretation of spectral sensitivity curves at long wavelengths. *J Physiol* 130(1):45–52.
8. Sliney DH, Wangemann RT, Franks JK, Wolbarsht ML (1976) Visual sensitivity of the eye to infrared laser radiation. *J Opt Soc Am* 66(4):339–341.
9. Dmitriev VG, et al. (1979) Nonlinear perception of infra-red radiation in the 800-1355 nm range with human eye. *Sov J Quantum Electron* 9(4):475–479.
10. Walraven PL, Leebeek HJ (1963) Foveal sensitivity of the human eye in the near infrared. *J Opt Soc Am* 53:765–766.
11. Zaidi Q, Pokorny J (1988) Appearance of pulsed infrared light: Second harmonic generation in the eye. *Appl Opt* 27(6):1064–1068.
12. Denk W, Strickler JH, Webb WW (1990) Two-photon laser scanning fluorescence microscopy. *Science* 248(4951):73–76.
13. Gray-Keller M, Denk W, Shraiman B, Detwiler PB (1999) Longitudinal spread of second messenger signals in isolated rod outer segments of lizards. *J Physiol* 519(Pt 3):679–692.
14. Euler T, et al. (2009) Eyecup scope—optical recordings of light stimulus-evoked fluorescence signals in the retina. *Pflugers Arch* 457(6):1393–1414.
15. Kochendoefer GG, Mathies RA (1996) Spontaneous emission study of the femtosecond isomerization dynamics of rhodopsin. *J Phys Chem* 100(34):14526–14532.
16. Curcio JA, Petty CC (1951) The near infrared absorption spectrum of liquid water. *J Opt Soc Am* 41(5):302–304.
17. Snyder AW, Pask C (1973) The Stiles-Crawford effect—Explanation and consequences. *Vision Res* 13(6):1115–1137.
18. Boettner EA, Wolter JR (1962) Transmission of the ocular media. *Invest Ophthalmol Vis Sci* 1(6):776–183.
19. Heywood CA, Kentridge RW (2003) Achromatopsia, color vision, and cortex. *Neurol Clin* 21(2):483–500.
20. Palczewska G, et al. (2010) Noninvasive multiphoton fluorescence microscopy resolves retinol and retinal condensation products in mouse eyes. *Nat Med* 16(12):1444–1449.
21. Han M, Giese G, Bille J (2005) Second harmonic generation imaging of collagen fibrils in cornea and sclera. *Opt Express* 13(15):5791–5797.
22. Vinberg F, Kolesnikov AV, Kefalov VJ (2014) Ex vivo ERG analysis of photoreceptors using an in vivo ERG system. *Vision Res* 101:108–117.
23. Heikkinen H, Nymark S, Koskelainen A (2008) Mouse cone photoresponses obtained with electroretinogram from the isolated retina. *Vision Res* 48(2):264–272.
24. Govardovskii VI, Fyhrquist N, Reuter T, Kuzmin DG, Donner K (2000) In search of the visual pigment template. *Vis Neurosci* 17(4):509–528.
25. Krispel CM, et al. (2006) RGS expression rate-limits recovery of rod photoresponses. *Neuron* 51(4):409–416.
26. Chang B, et al. (2006) Cone photoreceptor function loss-3, a novel mouse model of achromatopsia due to a mutation in Gnat2. *Invest Ophthalmol Vis Sci* 47(11):5017–5021.
27. Calvert PD, et al. (2001) Phototransduction in transgenic mice after targeted deletion of the rod transducin alpha-subunit. *Proc Natl Acad Sci USA* 98(18):10515–10515.
28. Humphries MM, et al. (1997) Retinopathy induced in mice by targeted disruption of the rhodopsin gene. *Nat Genet* 15(2):216–219.
29. Imamoto Y, Seki I, Yamashita T, Shichida Y (2013) Efficiencies of activation of transducin by cone and rod visual pigments. *Biochemistry* 52(17):3010–3018.
30. Ramon E, Mao X, Ridge KD (2009) Studies on the stability of the human cone visual pigments. *Photochem Photobiol* 85(2):509–516.
31. Kefalov VJ, et al. (2005) Breaking the covalent bond—a pigment property that contributes to desensitization in cones. *Neuron* 46(6):879–890.
32. Salom D, et al. (2006) Crystal structure of a photoactivated deprotonated intermediate of rhodopsin. *Proc Natl Acad Sci USA* 103(44):16123–16128.
33. Padayatti P, Palczewska G, Sun W, Palczewski K, Salom D (2012) Imaging of protein crystals with two-photon microscopy. *Biochemistry* 51(8):1625–1637.
34. McBee JK, Van Hooser JP, Jang GF, Palczewski K (2001) Isomerization of 11-cis-retinoids to all-trans-retinoids in vitro and in vivo. *J Biol Chem* 276(51):48483–48493.
35. He M, et al. (2013) Isolation of the retinal isomers from the isomerization of all-trans-retinal by flash countercurrent chromatography. *J Chromatogr A* 1271(1):67–70.
36. Salek P, et al. (2003) Calculations of two-photon absorption cross sections by means of density-functional theory. *Chem Phys Lett* 374(5-6):446–452.
37. González-Luque R, et al. (2000) Computational evidence in favor of a two-state, two-mode model of the retinal chromophore photoisomerization. *Proc Natl Acad Sci USA* 97(17):9379–9384.
38. Röhrig UF, Guidoni L, Rothlisberger U (2002) Early steps of the intramolecular signal transduction in rhodopsin explored by molecular dynamics simulations. *Biochemistry* 41(35):10799–10809.
39. Birge RR (1990) Photophysics and molecular electronic applications of the rhodopsins. *Annu Rev Phys Chem* 41:683–733.
40. Kecik D, Kasprzak J, Zajac A (2011) Perseption of laser radiation for near infrared range. *Acta Phys Pol* 120(4):686–687.
41. Xu C, Webb WW (1996) Measurement of two-photon excitation cross sections of molecular fluorophores with data from 690 to 1050 nm. *J Opt Soc Am B* 13(3):481–491.
42. Xu C, Zipfel W, Shear JB, Williams RM, Webb WW (1996) Multiphoton fluorescence excitation: New spectral windows for biological nonlinear microscopy. *Proc Natl Acad Sci USA* 93(20):10763–10768.
43. Koenig D, Hofer H (2011) The absolute threshold of cone vision. *J Vis* 11(1).

44. Kiser PD, Golczak M, Palczewski K (2014) Chemistry of the retinoid (visual) cycle. *Chem Rev* 114(1):194–232.
45. Gozem S, Schapiro I, Ferré N, Olivucci M (2012) The molecular mechanism of thermal noise in rod photoreceptors. *Science* 337(6099):1225–1228.
46. Delori FC, Webb RH, Sliney DH; American National Standards Institute (2007) Maximum permissible exposures for ocular safety (ANSI 2000), with emphasis on ophthalmic devices. *J Opt Soc Am A Opt Image Sci Vis* 24(5):1250–1265.
47. McConnell G (2006) Improving the penetration depth in multiphoton excitation laser scanning microscopy. *J Biomed Opt* 11(5):054020.
48. Lem J, et al. (1999) Morphological, physiological, and biochemical changes in rhodopsin knockout mice. *Proc Natl Acad Sci USA* 96(2):736–741.
49. Nymark S, Haldin C, Tenhu H, Koskelainen A (2006) A new method for measuring free drug concentration: Retinal tissue as a biosensor. *Invest Ophthalmol Vis Sci* 47(6):2583–2588.
50. Nymark S, Heikkinen H, Haldin C, Donner K, Koskelainen A (2005) Light responses and light adaptation in rat retinal rods at different temperatures. *J Physiol* 567(Pt 3):923–938.
51. Palczewski K, et al. (2000) Crystal structure of rhodopsin: A G protein-coupled receptor. *Science* 289(5480):739–745.
52. Neri M, Vanni S, Tavernelli I, Rothlisberger U (2010) Role of aggregation in rhodopsin signal transduction. *Biochemistry* 49(23):4827–4832.
53. Cornell WD, et al. (1995) A 2nd generation force-field for the simulation of proteins, nucleic acids, and organic molecules. *J Am Chem Soc* 117(19):5179–5197.
54. Wang J, Wolf RM, Caldwell JW, Kollman PA, Case DA (2004) Development and testing of a general amber force field. *J Comput Chem* 25(9):1157–1174.
55. Schulz R, Vargiu AV, Collu F, Kleinekathöfer U, Ruggerone P (2010) Functional rotation of the transporter AcrB: Insights into drug extrusion from simulations. *PLOS Comput Biol* 6(6):e1000806.
56. Ryckaert JP, Ciccotti G, Berendsen HJC (1977) Numerical integration of Cartesian equations of motion of a system with constraints: Molecular dynamics of N-alkanes. *J Comput Phys* 23(3):327–341.
57. Sulpizi M, et al. (2003) Reaction mechanism of caspases: Insights from QM/MM Car-Parrinello simulations. *Proteins* 52(2):212–224.
58. Martinez GR, et al. (2000) Peroxynitrite does not decompose to singlet oxygen ((1)Delta (g)O(2)) andnitroxyl (NO(-)). *Proc Natl Acad Sci USA* 97(19):10307–10312.
59. Sulpizi M, Schelling P, Folkers G, Carloni P, Scapozza L (2001) The rational of catalytic activity of herpes simplex virus thymidine kinase. a combined biochemical and quantum chemical study. *J Biol Chem* 276(24):21692–21697.
60. Laio A, VandeVondele J, Rothlisberger U (2002) A Hamiltonian electrostatic coupling scheme for hybrid Car-Parrinello molecular dynamics simulations. *J Chem Phys* 116(16):6941–6947.
61. Laio A, VandeVondele J, Rothlisberger U (2002) D-RESP: Dynamically generated electrostatic potential derived charges from quantum mechanics/molecular mechanics simulations. *J Phys Chem B* 106(29):7300–7307.
62. Martyna GJ, Klein ML, Tuckerman M (1992) Nose-Hoover chains: The canonical ensemble via continuous dynamics. *J Chem Phys* 97(4):2635–2643.
63. Hoover WG (1985) Canonical dynamics: Equilibrium phase-space distributions. *Phys Rev A* 31(3):1695–1697.
64. Nose S (1984) A unified formulation of the constant temperature molecular dynamics methods. *J Chem Phys* 81(1):511–519.
65. Car R, Parrinello M (1985) Unified approach for molecular dynamics and density-functional theory. *Phys Rev Lett* 55(22):2471–2474.
66. Yanai T, Tew DP, Handy NC (2004) A new hybrid exchange-correlation functional using the Coulomb-attenuating method (CAM-B3LYP). *Chem Phys Lett* 393(1-3):51–57.
67. Sneskov K, et al. (2013) Computational screening of one- and two-photon spectrally tuned channelrhodopsin mutants. *Phys Chem Chem Phys* 15(20):7567–7576.
68. Valsson O, Campomanes P, Tavernelli I, Rothlisberger U, Filippi C (2013) Rhodopsin absorption from first principles: Bypassing common pitfalls. *J Chem Theory Comput* 9(5):2441–2454.